Microporous and Mesoporous Materials 180 (2013) 71–78

Contents lists available at SciVerse ScienceDirect

Microporous and Mesoporous Materials

journal homepage: www.elsevier.com/locate/micromeso

Pore size distribution of ordered nanostructured carbon CMK-3 by means of experimental techniques and Monte Carlo simulations

Deicy Barrera, Mara Dávila, Valeria Cornette, J.C. Alexandre de Oliveira, Raúl H. López, Karim Sapag *

Laboratorio de Sólidos Porosos, Instituto de Física Aplicada, CONICET – Universidad Nacional de San Luis, Chacabuco 917, 5700 San Luis, Argentina

ARTICLE INFO

Article history:
Received 29 November 2012
Received in revised form 13 June 2013
Accepted 17 June 2013
Available online 28 June 2013

Keywords:
Nanostructured carbon
Pore size distribution
Grand canonical Monte Carlo

ABSTRACT

The design and study of new materials with specific properties is interesting in several scientific and technological fields. In the last years, nanostructured carbons (NC) have rapidly attracted the attention of some researchers due to their physicochemical properties useful for many applications among them in adsorption and catalysis.

In this work, the synthesis of a NC was carried out by a nanocasting method, using as a template a very ordered mesoporous material (SBA-15) and sucrose as carbon source. The final material consists of an ordered arrangement of parallel carbon nanorods bonded with some carbon nanowires (CMK-3 type), formed in the mesopores and micropores of the inorganic matrix. The inorganic matrix and the NC were structurally characterized by X-ray diffraction, texturally by N_2 sorption at 77 K, and morphologically by scanning electron microscopy. The Nitrogen experimental isotherms were simulated using Grand Canonical Monte Carlo (GCMC) method based on two kernels using slit and cylindrical pore models. From these models were obtained the pore size distributions (PSD) which were compared with those obtained by Quenched Solid Density Functional Theory (QSDFT) model. The GCMC simulation showed a good agreement with experimental adsorption isotherms and some differences with the corresponding pore size distribution obtained by Density Functional Theories Methods. These correlations validate the presented GCMC method as an alternative to study in detail the porosity of these materials.

1. Introduction

Energy and environmental problems have promoted the design of new materials to be used in more efficient processes. Nanostructured carbons (NC) have rapidly attracted the attention of researchers due to their physicochemical properties to be used in many applications as: separation processes (CH_4/CO_2 and N_2/O_2), gas storage (CH_4 and H_2), gas capture (CO_2) [1], energy storage as electrodes in lithium batteries [2,3] and electrochemical double-layer capacitors [4,5].

Unlike the traditional methods to synthesize carbon materials, a high control of porosity and ordered structure can be obtained using a nanocasting technique to produce novel materials. In this procedure, an inorganic porous material is chosen as a template and is impregnated with a carbon precursor (as sucrose, furfuryl alcohol, acetylene, etc.). Then, this composite is dried and pyrolyzed and the template is removed by hydrofluoric acid or sodium hydroxide leaching. Different templates like porous silica, zeolites, pillared clays, are used to obtain carbons with a variety of structures and pore sizes. Jun et al. [6] synthesized with this technique the first nanostructured carbon CMK-3 type. They used an ordered mesoporous material (SBA-15) as a template and sucrose as a carbon source. The resulting material was an exact negative replica of the SBA-15 porous structure formed by parallel interconnected carbon nanorods. This material became attractive due to its interesting textural, structural and morphological properties. In comparison with the corresponding template the synthesized carbon material exhibits a more hydrophobic nature, excellent mechanical strength and thermal stability, making it even more attractive for many applications [7–9].

The standard method used to characterize the texture of ordered mesoporous materials (OMM) is by the N_2 adsorption–desorption isotherms at 77 K [10–12]. In addition to these experimental analyses there are many theoretical and simulation studies that attempt to complete the characterization of these kinds of materials using the adsorption data. Particularly, the interest was focused on obtaining the Pore Size Distribution (PSD) of these materials.

In the last years, an important progress has been achieved using molecular theories to calculate the PSD of different materials where the most popular methods are supported by the Density Functional Theory, as the Non-Local Density Functional Theory (NLDFT) [13–15]. NLDFT method is a reliable and useful tool to study classical inhomogeneous fluids. This method describes the

* Corresponding author. Tel.: +54 2664 4520300x6135; fax: +54 2664 452300x6135.
E-mail address: sapag@unsl.edu.ar (K. Sapag).

1387-1811/$ - see front matter © 2013 Elsevier Inc. All rights reserved.
http://dx.doi.org/10.1016/j.micromeso.2013.06.028

structure of simple confined fluids in simple confining geometries such as slits, spheres, cylinders (as is the case of SBA-15 materials) and hybrids [16,17]. NLDFT neglects the influence of connectivity in the pore model and assumes that the surface is smooth and rigid and that no surface functional groups are present, disregarding corrugation effects, swelling, and chemical heterogeneity. The fluid–fluid and solid–fluid parameters of the Lennard–Jones potentials are used to represent different adsorption systems [18,19]. This method produces some inaccuracies in carbons with heterogeneous surfaces and disordered pore structure. To overcome this problem, Gor et al. [20] presented an advanced NLDFT method named Quenched Solid Density Functional Theory (QSDFT), where the system is modeled using a distribution of solid atoms rather than a source of the external potential field. This fact, allows take into account the heterogeneity effects in carbons due to the surface roughness, improving the previous NLDFT that assumes flat, structureless and graphitic pore walls. This method was developed to obtain the pore size distribution taken into account the geometrical and chemical characteristics of micro-mesoporous carbons, in the range from 0.4 to 50 nm. The calculated theoretical isotherms (kernels) were developed for cylindrical, slit, and a mixture of these pore geometries. In the last one slit geometries are only considered for the micropores and cylindrical for the mesopores range [20]. These DFT methods (NLDFT and QSDFT) were developed and implemented in commercial sorption instruments.

Among the molecular methods, the Grand Canonical Monte Carlo (GCMC) simulation is also appropriate to be applied in the study of porous materials. GCMC was used for several authors [21,22] to model the adsorption process in CMK-3 type material obtaining reliable results. An interesting point to explore, which has not been developed by these authors, is the use of this methodology to obtain the PSD of these materials.

In the present work, the synthesis and characterization of an ordered mesoporous carbon type CMK-3 were carried out by different experimental techniques and Monte Carlo simulation. The CMK-3 was characterized using X-ray diffraction (XRD), scanning electron microscopy (SEM) and nitrogen adsorption–desorption measurements, with the aim of evaluating their structural, textural and morphological properties. By Monte Carlo simulations two set of isotherms (kernel) were built based on slit and cylindrical pores in the Grand Canonical ensemble. From the experimental data, and the kernels obtained by GCMC, the PSDs were plotted and compared with those obtained by QSDFT method implemented into Quantachrome's data reduction software.

2. Experimental

2.1. Materials

Reagents used in these syntheses include the surfactant Pluronic P123 triblock copolymer (EO_{20}-PO_{70}-E_{20}) (Aldrich); tetraethyl orthosilicate (TEOS 98%) (Merck); hydrochloric acid (Merck); sulfuric acid (Merck); hydrofluoric acid (Merck); sucrose (Biopack) and deionized water.

2.1.1. Synthesis of template

An ordered mesoporous material, SBA-15, was synthesized under non-hydrothermal conditions [23] in order to use it as a template in the obtaining of the nanostructured carbon. The molar ratio used for the preparation of the SBA-15 was: **0,017***P123*:**1***TEOS*:**6***HCl*:**140***H_2O*. Pluronic P123 was dissolved in a 2 M aqueous solution of HCl and kept under stirring at 40 °C for 3 h. TEOS was drop-wise added to the solution, which was vigorously stirred at the same temperature for 4 h. This reaction mixture was aged at 40 °C for 20 h without stirring. Afterwards, the temperature was raised to 80 °C and maintained for 48 h. The resultant solid material was filtered and washed with deionized water until reaching a conductivity value smaller than 10 S/cm. Subsequently, the material was dried at 60 °C for 12 h and calcined at 550 °C for 6 h at 1 °C/min.

2.1.2. Synthesis of nanostructured carbon

The synthesis of the nanostructured carbon, type CMK-3, was performed based on different reported conditions [6,24,25]. The synthesis involves four main steps: (i) impregnation of the template with the organic precursor; (ii) polymerization; (iii) pyrolysis and, (iv) template removal. The synthesis was carried out using SBA-15 as a template and sucrose as carbon source. SBA-15 was impregnated with an aqueous solution of sucrose dissolved in sulfuric acid and water in a mass ratio of 1:1.3:0.14:5 (SBA-15:Sucrose:H_2S0_4:H_2O). The mixture was stirred at room temperature for 1 h and then it was dried at 100 °C for 6 h. Subsequently, the temperature was raised to 160 °C for 6 h. The resultant dark brown colored composite was impregnated a second time with a mixture of aqueous solution of sucrose, sulfuric acid and water with a mass ratio of 0.8:0.09:5. This composite was treated again at the same drying conditions to complete the polymerization step. The pyrolysis process was carried out by heating the mixture from room temperature (RT) up to 900 °C, in a N_2 flow of 180 ml/min with a heating rate of 3 °C/min. The final temperature was keeping for 6 h and then is cooling up to RT. The nanostructured carbon was recovered by leaching the mesoporous framework in a 5 wt.% hydrofluoric solution at RT for 24 h. The obtained carbon, without template, was filtered and washed several times with deionized water and ethanol (50:50% v/v) until the conductivity value was smaller than 10 S/cm. Finally, the nanostructured carbon was overnight dried at 80 °C. Fig. 1 shows a scheme of the geometrical structure and formation of the CMK-3 material.

2.2. Characterization

The structural characteristics of the template and the nanostructured carbon material were obtained from small angle X-ray diffraction (XRD) measurements in an X'Pert PRO MPD Philips diffractometer using Cu Kα radiation from 1 to 5° of 2θ. Scanning electron microscopy (SEM) images were taken on a LEO 1450VP, equipped with an Energy Dispersive Spectrometer (EDS) Analyzer, Genesis 2000. Measurements of N_2 (99.999%) adsorption–desorption isotherms at 77 K were carried out using a volumetric adsorption apparatus (AUTOSORB-1MP, Quantachrome Instruments). Samples were previously degassed at 150 °C for 12 h, up to residual pressure was smaller than 0.5 Pa.

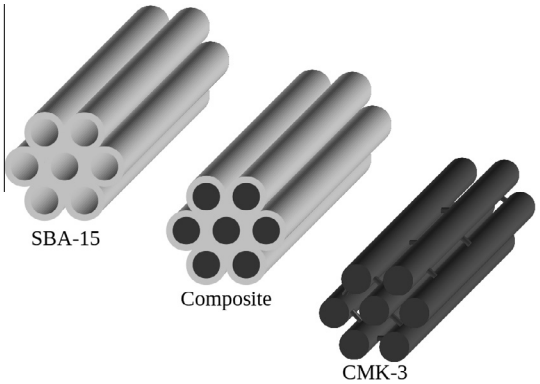

Fig. 1. Schematic structure of SBA-15 and CMK-3.

2.3. Calculations

The specific surface area (S_{BET}) of the SBA-15 and CMK-3 samples was estimated with the Brunauer, Emmet and Teller (BET) method [26], using the adsorption data in the range of relative pressures from 0.05 to 0.18 and 0.05 to 0.22 for the SBA-15 and CMK-3 samples, respectively, where the conditions of linearity and considerations regarding the method were fulfilled [12]. The total pore volume (V_{TP}) was obtained by the Gurvich's rule at a relative pressure of 0.98 [11]. The α-plot method [12,27] was used to calculate the micropores volume ($V_{\mu P}$) using the LiChrospher Si-1000 macroporous silica gel [28] and GCB-I [29] as the reference adsorbents for SBA-15 and CMK-3, respectively. The pore size distribution of the samples were obtained by the Quantachrome software, using NLDFT method for the SBA-15 (*using kernel for N_2 at 77 K on silica, cylindrical pores, NLDFT equilibrium model*) and the QSDFT method for the CMK-3 sample (*with the kernel for N_2 at 77 K on carbon, cylindrical pores, adsorption branch; N_2 at 77 K on carbon, slit pore, equilibrium model and N_2 at 77 K on carbon, slit/cylindrical pores, adsorption branch*). Once the adequate kernel is selected, the software constructs simulated isotherms which fit to the experimental ones, varying the relative weight of the local isotherms corresponding to each pore size. The PSD is obtained from the isotherms for each pore size and its relative contribution to adjust the experimental isotherm, corresponding to solve the integral adsorption equation [20].

3. Molecular simulation

3.1. Pore structure and interaction potential models

The Grand Canonical Monte Carlo (GCMC) simulation [30,31] was adopted to study the adsorption behavior of gases in the CMK-3 material. The proposed model considers the interstitial space between the nanorods as a collection of independent cylindrical or slit pores or a mixture of them, with different sizes. The assumption is that adsorption occurs only on the internal space of these pores.

The slit pores are built by two parallel walls of graphene layers. The pore size is defined as the distance between the two planes passing through the centers of carbon atoms in the first layers of the pore walls, leading to its interior.

The interaction energy between a fluid particle (nitrogen) and a single pore wall at a distance z (measured between the center of the fluid atom and the atoms in the outer layer of the solid) was obtained by the superposition of two Steele potentials, one per each infinite plate:

$$U_{gs-STEELE}(z) = 2\pi\varepsilon_{gs}\rho_C\sigma_{gs}^2\Delta\left\{\frac{2}{5}\left(\frac{\sigma_{gs}}{z}\right)^{10} + \left(\frac{\sigma_{gs}}{z}\right)^{4} - \frac{\sigma_{gs}^4}{3\Delta(z+0.61\Delta)^3}\right\} \quad (1)$$

where Δ is the separation between the graphite layers (0.335 nm), ρ_C is the density, number of carbon atoms per unit volume of graphite (114 nm^{-3}), and ε_{gs} and σ_{gs} are the solid–fluid Lennard–Jones parameters.

For the cylindrical geometry, the pore walls are made with wrapped graphene layers. The pore size is defined as the diameter of a ring passing through the centers of the carbons in the first layer of the pore wall.

A simplified treatment of the adsorbent-adsorbate interactions based upon the potential of a homogeneous cylindrical surface with effective parameters is used. Interactions with the adsorbent are modeled using the form of the Lennard–Jones potential integrated over an infinitely long cylinder [32,33].

$$u^{sf}(r,R) = \rho_{surf}\varepsilon_{sf}(\sigma_{sf}^{12}I_{12} - \sigma_{sf}^{6}I_6) \quad (2)$$

where:

$$I_{12} = \frac{63\pi^2}{32r^{10}(2-r/R)^{10}}F\left(-\frac{9}{2},-\frac{9}{2};1;(1-r/R)^2\right)$$

$$I_6 = \frac{3\pi^2}{r^4(2-r/R)^4}F\left(-\frac{3}{2},-\frac{3}{2};1;(1-r/R)^2\right)$$

and ρ_{surf} is a two-dimensional density of a carbon cylinder, $F(\alpha,\beta;Y;X)$ is an hypergeometric function, σ_{sf} and ε_{sf} are the size and energy parameters in the Lennard–Jones (LJ) potential between an adsorbed molecule and a carbon atom, calculated by the Lorentz-Berthelot rules using the parameter values shown in Table 1. The intermolecular interaction between the adsorbed molecules, $\phi_{ff}(r_{ij})$, is modeled using LJ potential (Eq. (3)).

$$\phi_{ff}(r_{ij}) = 4\varepsilon_{ff}\left[\left(\frac{\sigma_{ff}}{r_{ij}}\right)^{12} - \left(\frac{\sigma_{ff}}{r_{ij}}\right)^{6}\right] \quad (3)$$

where, r_{ij} is the intermolecular separation, ε_{ff} and σ_{ff} are LJ parameters of fluids. The LJ parameters of nitrogen are listed in Table 1.

A collection of adsorption isotherms (the local isotherms, θ_L) was obtained through the GCMC method, following the algorithm outlined in Ref. [30,31], both for the slit and the cylindrical geometries with the interaction potentials described above. Transition probabilities for each Monte Carlo attempt (displacement, adsorption and desorption of molecules), are given by the usual Metropolis rules. The lateral dimensions of the cell for the slit geometry and the longitudinal dimension for cylindrical geometry were taken as 50 nm, where the periodic boundary conditions were used in those directions. Equilibrium was generally achieved after 2×10^7 MC attempts, after which mean values were taken over the following 10^7 MC attempts for configurations spaced by 10^3 MC attempts, in order to ensure statistical independence. This collection of isotherms was used in three ways to fit a given experimental isotherm: (a) pure slit pores (PSG); (b) pure cylindrical pores (PCG) and (c) a mixture of slit and cylindrical pores (MSCG), with an undetermined fraction x of slit pores.

The accessible pore volume is defined as the space available to the center of an adsorbate molecule where the solid–fluid potential is negative [34,35]. Thus, the adsorption excess (and therefore the adsorption isotherm) may be calculated.

3.2. Calculating the pore-size distribution

Davies and Seaton [36–38] have addressed the problem of calculating PSDs from adsorption data in detail and the most important aspects of the solution procedure are presented in this work.

The experimental adsorption isotherm θ^{Exp} can be expressed as a superposition of isotherms corresponding to each pore size (H_j), pressure P and temperature T, called local isotherms, θ_L (obtained by GCMC simulation), with a weight corresponding to the pore-size distribution, $f(H_j)$:

Table 1
Values of Lennard–Jones and adsorbent parameters used in the simulation [30].

Specie	Parameter	Value
Nitrogen	σ_{ff}	0.3615 nm
	ε_{ff}/k_B	101.4 K
Carbon (adsorbent)	σ_{ff}	0.34 nm
	ε_{ff}/k_B	28 K
	ρ_{surf}	38.2 nm-2

$$\theta_i^{Exp} = \sum_{j=1}^{m} \theta_L(H_j^*, P_i, T) f(H_j^*) \delta H_j^* \quad (4)$$

where m is the number of quadrature intervals used in the analysis, and H^* is the mid-point of each quadrature interval. Eq. (4) cannot be directly solved due to the ill-posed and ill-conditioned properties of these equations. However, the detrimental effect of both properties can be minimized by employing regularization. The PSD is then obtained by fitting Eq. (4) plus the regularization term numerically, as proposed by Davies and co-workers, via a fast non-negative least-square algorithm. This is the most commonly used method to stabilize the result, incorporating additional constraints that are based on the smoothness of the PSD [37–39]. Physically, this corresponds to recognizing that a real PSD is more likely to be relatively smooth and centered around a few dominant pore sizes, rather than being highly fragmented and spiky. One of the complicating factors when the regularization is employed is that it requires the identification of an optimal smoothing parameter to be used in the analysis. To overcome this difficulty, we have used L curves [37] to determine the optimal amount of smoothing. Such L curves are a plot of some measure of the error of fit to the data against the smoothing parameter. In general, the error of fit to the data increases as the value of the smoothing parameter increases. However, below a threshold value of the smoothing parameter the increase in the error is often negligible whilst above the threshold the error increases rapidly. PSD solutions satisfying minimum L-curve and generalized cross-validation criteria have been shown to have a superior predictive performance relative to other possible PSD solutions [37,38,40]. It is interesting that two PSDs, though different in shape, can give similar predictions that are in good agreement with the experimental isotherms [41]. The above mentioned idea suggests that several good PSDs in terms of their predictive abilities can exist, which represent the porous structure of a nanostructured carbon (although the real material has a unique PSD) [42].

Gusev and O'Brien [43] recognized that, for a given set of data, there is a maximum pore size that can be identified reliably in a PSD analysis. Differentiating large pores from one to another is difficult because the extent of adsorption is virtually indistinguishable from one pore to another. This arises when the adsorption onto the opposite walls of a single pore occurs essentially independently, i.e., the pore walls become too far away from each other to enhance adsorption. The pore size, moreover, depends on the adsorptive and it is a function of the temperature and the pressure. Since the adsorption in all the pores larger than those in the window of reliability is essentially indistinguishable, assigning a single quadrature interval to this region makes best use of the experimental data.

Based on the above mentioned, the PSD for slit and cylindrical pores have been calculated with kernels containing 48 pore sizes between 0.4 nm and 5.4 nm and between 1 nm and 6 nm respectively, both with 40 relative pressure points (5.0×10^{-4}–0.99).

The experimental isotherm was fitted with the PSG model, the PCG model, and with the MSCG model by using the same number of parameters (number of pore size intervals) in all of the cases.

The choice of the kernel for deriving the PSD for a given carbon sample should be made based on the a priori information about the adsorbent material [20]. A usual criterion for the choice of a certain MCGC kernel is the fitting of resulting PSD to the experimental isotherm. Improper choice of pore geometry usually leads to bad fitting results.

4. Results and discussion

4.1. Kernel of simulated isotherms

The kernel of selected GCMC adsorption isotherms (all were carried out at 77 K) for slit and cylindrical geometry are shown in Figs. 2 and 3. The isotherm shapes depend on the pore size and are smooth prior to the capillary condensation steps, which are characteristic to mesopores (>2 nm), and do not exhibit stepwise inflections caused by artificial layering transitions. This layering is an artifact caused by the use of the simplified, structure-less pore wall model and approximations made in the theory.

4.2. Characterization of the samples

Fig. 4 shows the powder XRD patterns of SBA-15 and CMK-3 materials. The SBA-15 diffractogram exhibits three well-resolved peaks that can be indexed as the spaces of 100, 110, and 200 planes and are associated to *p6mm* space group. The CMK-3 sample presents a difractogram with a clear peak corresponding to the 100 plane, characteristic of these kinds of ordered mesoporous carbons [44]. The patterns for both samples suggest that they are ordered mesoporous materials with well-defined pore geometry and narrow PSD. The d_{100} plane for the CMK- 3 sample is minor than the SBA-15 sample, denoting the contraction in the structure after the synthesis process.

Fig. 5 shows the rod-like morphology present in all SBA-15 and CMK-3 materials. Both materials present similar morphologies with uniform micrometer rod-like particles in concordance with

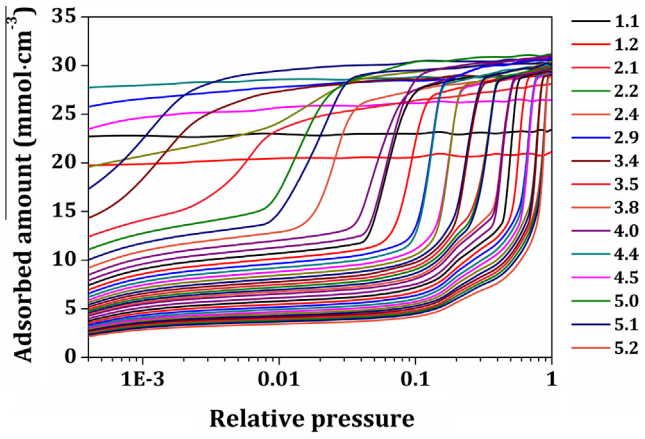

Fig. 2. Selection of simulated adsorption isotherms, for nitrogen at 77 K using slit pore model (in the right side are shown the labels of the pore sizes in nm).

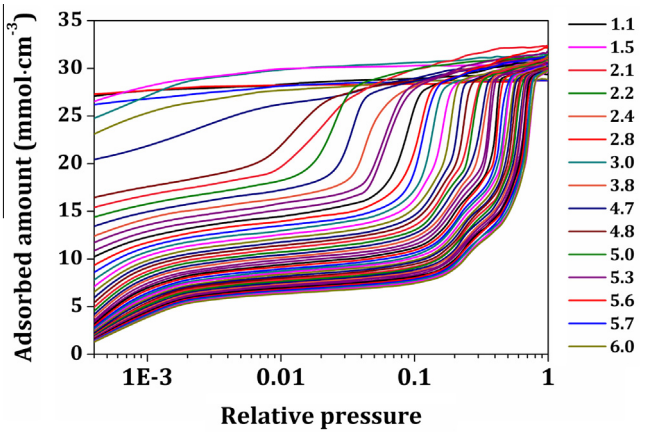

Fig. 3. Selection of simulated adsorption isotherms, for nitrogen at 77 K using cylindrical pore model (in the right side are shown the labels of the pore sizes in nm).

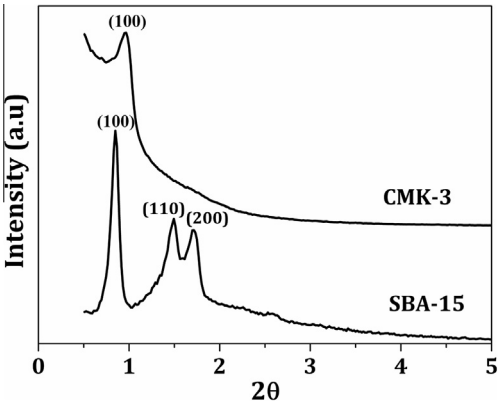

Fig. 4. X-ray diffraction patterns of SBA-15 and CMK-3.

other ones reported previously [45,46]. It can be seen that the order in the template structure was maintained. Chemical analysis (by EDS) of these structures showed that the template has only Si and the CMK-3 sample has only carbon, confirming the success of the synthesis and the order of the samples.

Fig. 6(a) shows the experimental nitrogen adsorption–desorption isotherms at 77 K of the SBA-15 and CMK-3 materials. CMK-3 sample exhibits capillary condensation steps at 0.45 in relative pressures. Both kinds of materials exhibited Type IV isotherms

Table 2
Textural properties of SBA-15 and CMK-3 materials.

Material	Specific surface area ($m^2\ g^{-1}$)	$V_{\mu P}$ ($cm^3\ g^{-1}$)	V_{TP} ($cm_3\ g^{-1}$)
SBA-15	850 (BET)	0.06	1.10
CMK-3	1300 (BET)	0.15	1.12

which are typical for mesoporous structures [6,24,39]. In the case of the SBA-15, the adsorption and desorption branches in the hysteresis loops are parallel (Type H1 loop according to the IUPAC classification [12]), which is typical of materials with cylindrical geometries and uniform pore sizes. This material adsorbs at very low pressures ($p/p_0 < 0.05$), which is due to the micropore filling (or strong adsorbate–adsorbent interactions) while the adsorption at higher relative pressures ($0.05 < p/p_0 < 0.7$) may be attributed to mono-multi-layer adsorption of nitrogen on mesopore walls with the consequent capillary condensation. In the CMK-3 material the hysteresis loop has some H2 type characteristics where the desorption branch is much steeper than the adsorption branch. This behavior should be due to the pore blocking affecting the pressure where the pore evaporation/desorption occurs. Therefore, for this material the PSD must be calculated from the adsorption branch of the isotherm (where pore blocking effects are not present).

Fig. 6(b) shows the pore size distribution obtained for SBA-15 and CMK-3 materials using NLDFT and QSDFT methods for

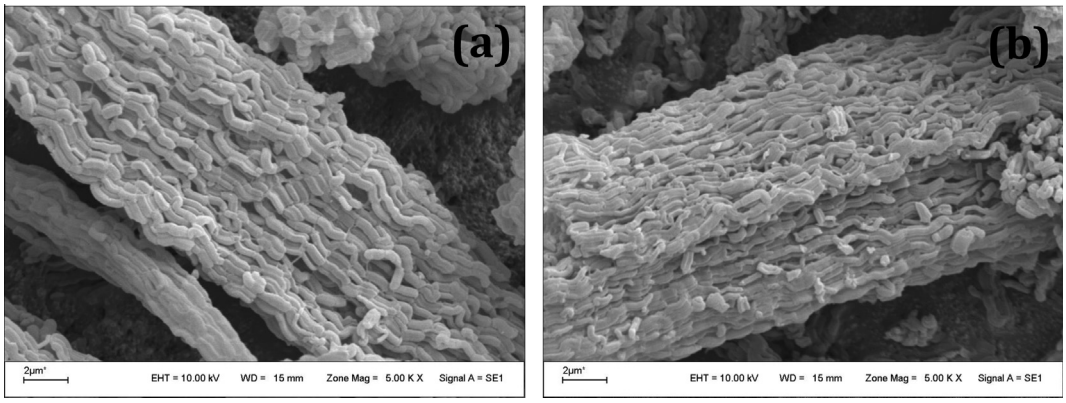

Fig. 5. SEM images of (a) SBA-15 and (b) CMK-3.

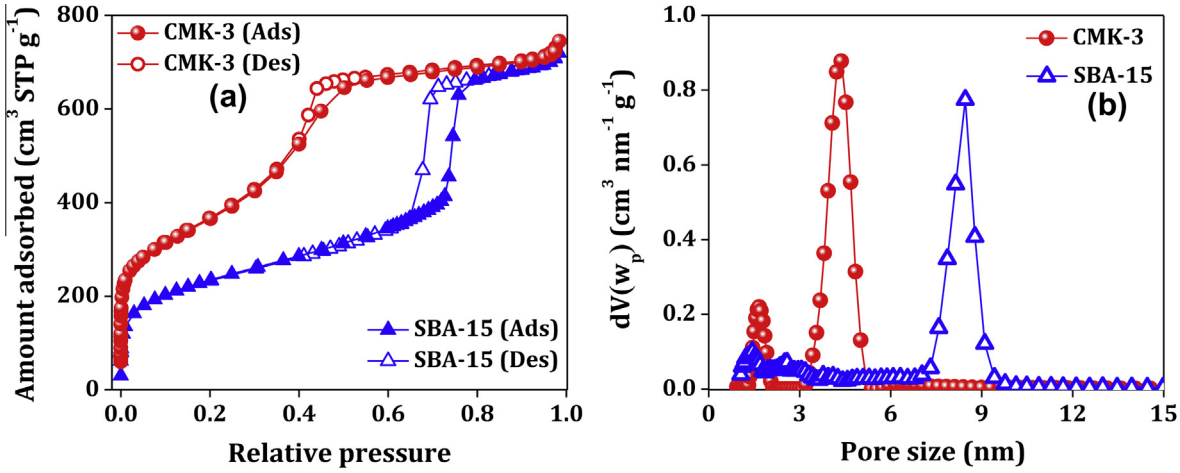

Fig. 6. (a) Nitrogen adsorption–desorption isotherm at 77 K and (b) pore size distribution of the samples SBA-15 using NLDFT; and CMK-3 using QSDFT methods. (both PSD were obtained by using cylindrical kernels from Quantachrome's software).

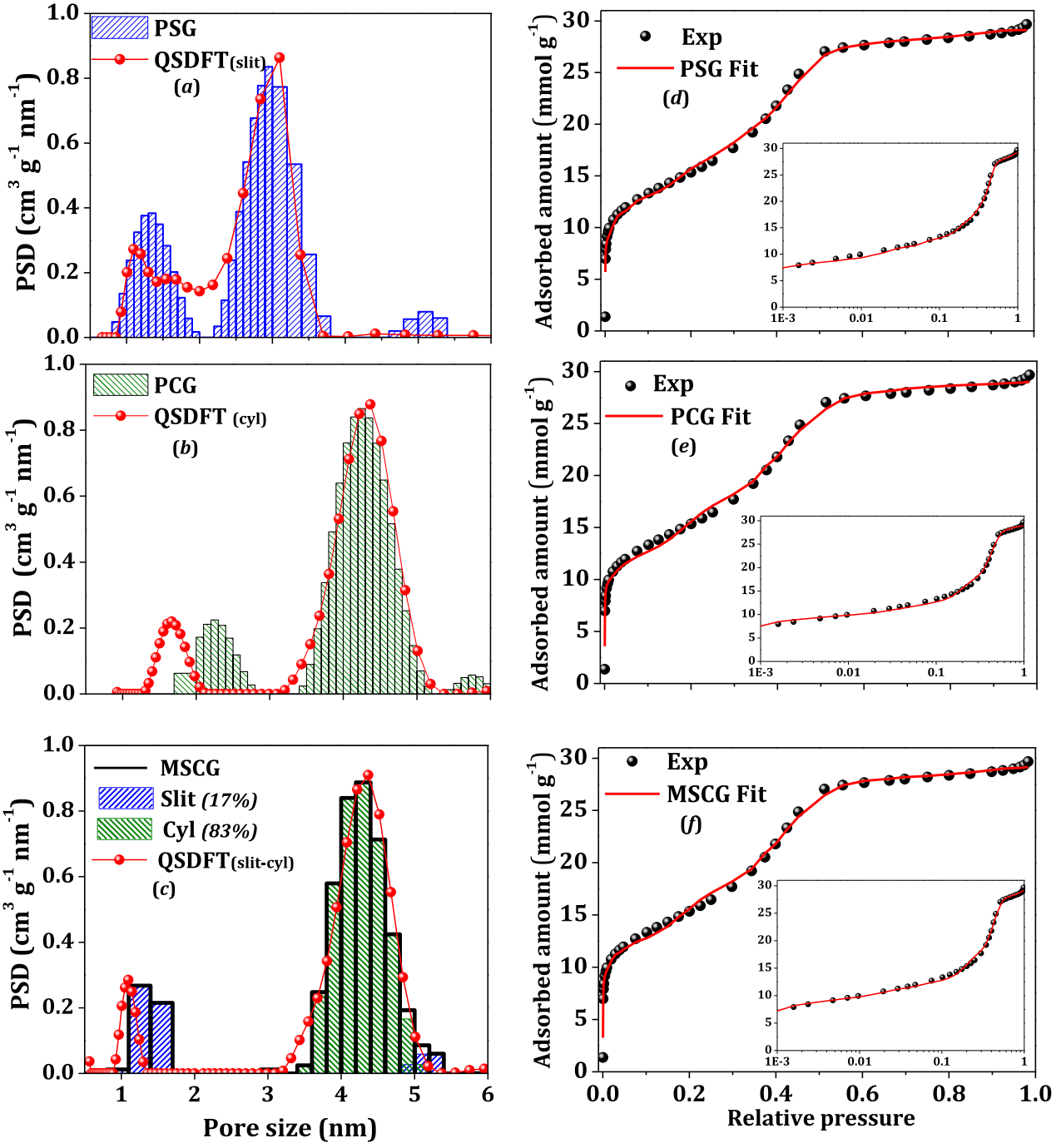

Fig. 7. Comparison between PSDs obtained by: (a) QSDFT with slit pore and PSG model, (b) QSDFT with cylindrical pore and PCG model and (c) QSDFT with slit-cylindrical pores and MSCG slit – cylindrical model. Fitting curves between the experimental and simulated N_2 adsorption isotherms of CMK-3 using: (d) PSG, (e) PCG and (f) MSCG kernels. Adsorption isotherms in logarithmic pressure scales are shown in the inset.

cylindrical geometries, respectively. These materials present a narrow bimodal pore size distribution with pores in the microporous and mesoporous region. For both samples the micropores are around 1.5 nm, but the mesopore sizes are different being centered at 8.4 nm for the SBA-15 and at 4.4 nm for the CMK 3 type sample, where this reduction is according to XRD analysis. The presence of mesopores is consistent with what was expected of this type of sample, but the micropores origin is not clear and it has not been widely studied.

Table 2 shows the textural properties for both materials where S_{BET} is the specific surface area, $V_{\mu P}$ the micropore volume calculated by α_s-plot method and V_{TP} is the total volume pore obtained by Gurvich's rule. It could be seen that the nanostructured carbon (CMK-3) presents higher values than SBA-15 in all of these properties, consistent with results observed in Fig. 6.

In Fig. 7 are shown the PSD from the experimental isotherm derived from the three GCMC kernels, slit (PSG), cylindrical (PCG) and mixed (MSCG), in comparison with that obtained from the equipment software (QSDFT). In the right side of the Fig. 7(d–f) the fits of the experimental isotherms obtained by Monte Carlo methods are shown. As a first general observation, the three PSDs have a bimodal distribution from Monte Carlo and QSDFT method.

In Fig. 7(a) can be observed that using the pure slit geometry model a peak near at 3 nm in the mesoporous region is present in both models (QSDFT and MC). This value is quite different to the expected ones by XRD for these materials (near 4.5 nm), supposing a hexagonal array of nanorods in the place of cylinder pores in SBA-15. This fact could be evidence that the slit model is not suitable in the mesoporous region. However, the fitting of the experimental isotherm using the PSG kernel shows a good agreement with the experimental data as is shown in Fig. 7(d). It is a remarkable fact to have into account that a good fit of the model is not enough to conclude about the best PSD. In the micropores region both methods using slit pores geometries are in agreement, although the PSD obtained by MC is more defined in this region. Additionally the MC method shows pores larger than 5 nm, which is possible to assign to secondary mesoporosity from not ordered regions of the sample or to the porosity between nanorods in the region where nanowires are. Also, it is possible assign this fact to an artifact of the fitting procedure, by the similarity between the slit and cylindrical simulated isotherms for size larger than 4 nm.

In the PSD from the PCG and QSDFT for cylindrical geometries, (Fig. 7(b)) a single sharp peak can be distinguished in the mesopores range in agreement with that obtained by the X-ray data. In the other region (smaller pores) there is no agreement between them even more, the MC methods for cylindrical geometry do not detect micropores in this region. Zhou et al. [3] reported that CMK-3 includes a small amount of stacked crystalline graphite phase and Jun et al. [6] that the pore walls are constructed by disordered carbon networks similar to activated carbons. Then, the origin of the microporosity observed in the PSD can be attributed to small and quite disordered hollows inside the carbon nanorods and the slit geometry model, in this case, is more appropriate. This is in accordance with the results obtained by PCG method. Fig. 7(e) shows the adjustment of the experimental isotherm using the Monte Carlo method.

In Fig. 7(c) is shown the PSD using a mixture of slit and cylindrical geometries for MC and DFT methods. Fig. 7(f) shows the adjustment of the experimental isotherm using the Monte Carlo method. In the PSD showed in the Fig. 7(c), the QSDFT method is restrictive in the selection to adjust the experimental data, where the slit kernel is only used for the micropores region and the cylindrical for the mesoporous region. On the other hand, the Monte Carlo method uses a unique kernel composed by the isotherms obtained for both slit and cylindrical geometries for all pores range. The PSD obtained are similar for both methods, but the MSCG shows the exclusive contribution of the slit pores in the micropores region in agreement with the above mentioned, and a smaller contribution near mesopores larger about 5 nm, that can be associated to secondary porosity. In the mesoporous range, the MSCG model predicts a PSD formed mostly by cylindrical pores which agrees very well with QSDFT prediction, validating the proposed model.

Table 3 shows a comparison among the micropore volumes ($V_{\mu P}$), mesopore volumes (V_{mP}) and modal pore size (w_P) in the microporous and mesoporous regions, obtained for different methods. From these data is possible to observe a good agreement between MSCG and QSDFT (cyl-slit) methods.

Table 3
Textural properties obtained by the different studied methods considering the pore geometries.

CMK-3	$V_{\mu P}$ ($cm^3\ g^{-1}$)	V_{mP} ($cm^3\ g^{-1}$)	$w_{\mu P}$ (nm)	w_{mP} (nm)
αs-plot	0.15	0.71	–	–
QSDFT (slit)	0.25	0.73	1.2	3.1
QSDFT (cyl)	0.15	0.81	1.6	4.4
QSDFT (cyl-slit)	0.15	0.81	1.1	4.4
PSG	0.25	0.73	1.4	3.0
PCG	0.04	0.91	2.3	4.3
MSCG	0.15	0.81	1.3	4.3

5. Conclusions

For the experimental section, a SBA-15 type material and the corresponding mesoporous carbon CMK-3 type were successfully synthesized with an ordered structure formed by cylinders of pure silicon and nanorods of pure carbons respectively and were verified by XRD, N_2 adsorption–desorption isotherms, and SEM. The pore size distributions of the samples presented two well defined pore sizes, one of them in the mesopores and the other one in the micropores range. In SBA-15 material, according to reported by other authors, mesopores correspond to the inner of hexagonally ordered cylinder and the micropores to small channels connecting these mesopores. On the other hand, the mesopores in the CMK-3 sample correspond to the space between the nanorods and the micropores can be attributed to small hollows inside the carbon nanorods. These characteristics make this carbon material interesting to be applied in Adsorption and Catalysis.

The Monte Carlo simulation applied for different geometries produced simulated isotherms that can adjust very well the experimental isotherm in all of the cases. In front of QSDFT, from the GCMC model is possible to conclude that the CMK-3 texture can be modeled with cylindrical geometry for primary mesopores and slit geometries for the micropores and secondary mesopores. However, the textural data obtained by the GCMC method agrees with the obtained by the QSDFT method for the CMK-3 sample being a good alternative model.

Despite the simple geometry and not exact structure considered according to the known structure of the CMK-3 sample, the use of the GCMC method gives good results. These achievements indicate that it is the right way to study this kind of material, where further studies would be needed focused on improving the structural model.

Acknowledgments

This work was financially supported by UNSL, ANPCyT and CONICET (Argentina). Authors are also grateful to the research group of Prof. Rodriguez Castellón, from the University of Málaga, Spain for the XRD analysis.

References

[1] D. Saha, S.J. Deng, Colloid. Interf. Sci. 345 (2010) 402–409.
[2] P.G. Bruce, S.A. Freunberger, L.J. Hardwick, J.-M. Tarascon, Nat. Mater. 11 (2012) 19–29.
[3] H. Zhou, S. Zhu, M. Hibino, I. Honma, M. Ichihara, Adv. Mater. 15 (2003) 2107–2111.
[4] J. Zhang, L.-B. Kong, J.-J. Cai, Electrochim. Acta 55 (2010) 8067–8073.
[5] K. Xia, Q. Gao, J. Jiang, J. Hu, Carbon 46 (2008) 1718–1726.
[6] S. Jun, S.H. Joo, R. Ryoo, M. Kruk, M. Jaroniec, Z. Liu, T. Ohsuna, O. Terasaki, J. Am. Chem. Soc. 122 (2000) 10712–10713.
[7] A.-H. Lu, W.-C. Li, W. Schmidt, F. Schüth, Micropor. Mesopor. Mater. 80 (2005) 117–128.
[8] H.O. Pierson, Handbook of Carbon, Graphite, Diamond and Fullerenes – Properties Processing and Applications, William Andrew Publishing, 1993.
[9] G. Ertl, H. Knozinger, J. Weitkamp, Preparation of Solid Catalysts, WileyVCH, Germany, 1999.
[10] M. Thommes, Physical adsorption characterization of ordered and amorphous mesoporous materials, in: G.Q. Lu, X.S. Zhao (Eds.), Nanoporous Material. Science and Engineering, Imperial College Press, London, 2004, pp. 317–364.
[11] S.J. Gregg, K.S.W. Sing, Adsorption, Surface Area and Porosity, Academic Press, New York, 1982.
[12] F. Rouquerol, J. Rouquerol, K. Sing, Adsorption by Powders Porous Solids, Academic Press, San Diego, 1999.
[13] C.M. Lastoskie, K.E. Gubbins, Stud. Surf. Sci. Catal. 128 (2000) 41–50.
[14] P.I. Ravikovitch, G.L. Haller, A.V. Neimark, Adv. Colloid. Interf. 76–77 (1998) 203–226.
[15] A.V. Neimark, P.I. Ravikovitch, Stud. Surf. Sci. Catal. 128 (2000) 51–60.
[16] P.I. Ravikovitch, A.V.J. Neimark, Phys. Chem. B. 105 (2001) 6817–6823.

[17] P.M. Barata-Rodrigues, T.J. Mays, N.A. Seaton, G.D. Moggridge, Stud. Surf. Sci. Catal. 144 (2002) 139–146.
[18] P.I. Ravikovitch, A. Vishnyakov, A.V. Neimark, Rev. E. 64 (2001) 1–20.
[19] C. Lastoskie, K.E. Gubbins, N. Quirkeft, J. Phys. Chem. 97 (1993) 4786–4796.
[20] G.Y. Gor, M. Thommes, K.A. Cychosz, A.V. Neimark, Carbon 50 (2012) 1583–1590.
[21] M.W. Maddox, J.P. Olivier, K.E. Gubbins, Langmuir 13 (1997) 1737–1745.
[22] L.D. Gelb, K.E. Gubbins, Langmuir 15 (1999) 305–308.
[23] D. Barrera, J. Villarroel-Rocha, L. Marenco, M.I. Oliva, K. Sapag, Adsorpt. Sci. Technol. 29 (2011) 975–988.
[24] P. Srinivasu, A. Vinu, S. Hishita, T. Sasaki, K. Ariga, T. Mori, Micropor. Mesopor. Mat. 108 (2008) 340–344.
[25] M. Yang, Q. Gao, Micropor. Mesopor. Mat. 143 (2011) 230–235.
[26] S. Brunauer, P.H. Emmett, E.J. Teller, Am. Chem. Soc. 60 (1938) 309–319.
[27] A. Sayari, P. Liu, M. Kruk, M. Jaroniec, Chem. Mater. 9 (1997) 2499–2506.
[28] M. Jaroniec, M. Kruck, J. Olivier, Langmuir 15 (1999) 5410–5413.
[29] K. Nakai, M. Yoshida, J. Sonoda, Y. Nakada, H. Masako, H.J. Naono, Colloid. Interf. Sci. 351 (2010) 507–514.
[30] M.P. Allen, D.J. Tildesley, Computer simulation of liquids, Oxford University Press, New York, 1987.
[31] D. Frenkel, B. Smit, Understanding molecular simulations, Academic Press, New York, 2002.
[32] W.A. Steele, M.J. Bojan, Adv. Colloid. Interface. Sci. 76–77 (1998) 153–178.
[33] G.J. Tjatjopoulos, D.L. Feke, J.A. Mann, J. Phys. Chem. 92 (1988) 4006–4007.
[34] K. Kaneko, R.F. Cracknell, D. Nicholson, Langmuir 10 (1994) 4606–4609.
[35] T. Ohkubo, J. Miyawaki, K. Kaneko, R. Ryoo, N. Seaton, J. Phys. Chem. B 106 (2002) 6523–6528.
[36] G.M. Davies, N.A. Seaton, Carbon 36 (1998) 1473–1490.
[37] G.M. Davies, N.A. Seaton, V.S. Vassiliadis, Langmuir 15 (1999) 8235–8245.
[38] G.M. Davies, N.A. Seaton, AIChE J. 46 (2000) 1753–1768.
[39] M.V. Szombathely, P. Brauer, M.J. Jaroniec, Comput. Chem. 13 (1992) 17–32.
[40] J.M.C. Pinto Da Costa, R.F. Cracknell, N.A. Seaton, L. Sarkisov, Carbon 49 (2011) 445–456.
[41] A.A.G. Blanco, J.C.A. de Oliveira, R. López, J.C. Moreno-Piraján, L. Giraldo, G. Zgrablich, K. Sapag, Colloid. Surface. A 357 (2010) 74–83.
[42] Q. Cai, A. Buts, M.J. Biggs, N.A. Seaton, Langmuir 23 (2007) 8430–8440.
[43] V.Y. Gusev, J.A. O'Brien, N.A. Seaton, Langmuir 13 (1997) 2815–2821.
[44] S.H. Joo, R. Ryoo, M. Kruk, M. Jaroniec, J. Phys. Chem. B 106 (2002) 4640–4646.
[45] J. Roggenbuck, G. Koch, M. Tiemann, Chem. Mater. 18 (2006) 4151–4156.
[46] A.-H. Lu, F.C.R. Schüth, Chimie 8 (2005) 609–620.